J|A|C|S
ARTICLES
Published on Web 05/24/2007

Experimental and Theoretical Examination of C−CN and C−H Bond Activations of Acetonitrile Using Zerovalent Nickel

Tülay A. Ateşin,[†] Ting Li,[†] Sébastien Lachaize,[†] William W. Brennessel,[†] Juventino J. García,[‡] and William D. Jones*,[†]

Contribution from the Department of Chemistry, University of Rochester, Rochester, New York 14627, and Facultad de Química, Universidad Nacional Autónoma de México, México City, México, D.F. 04510

Received February 2, 2007; E-mail: jones@chem.rochester.edu

Abstract: Experimental and density functional theory show that the reaction of acetonitrile with a zerovalent nickel bis(dialkylphosphino)ethane fragment (alkyl = methyl, isopropyl) proceeds via initial exothermic formation of an η^2-nitrile complex. Three well-defined transition states have been found on the potential energy surface between the η^2-nitrile complex and the activation products. The lowest energy transition state is an η^3-acetonitrile complex, which connects the η^2-nitrile to a higher energy η^3-acetonitrile intermediate with an agostic C−H bond, while the other two lead to cleavage of either the C−H or the C−CN bonds. Gas-phase calculations show C−CN bond activation to be endothermic, which contradicts the observation of thermal C−CN activation in THF. Therefore, the effect of solvent was taken into consideration by using the polarizable continuum model (PCM), whereupon the activation of the C−CN bond was found to be exothermic. Furthermore the C−CN bond activation was found to be favored exclusively over C−H bond activation due to the strong thermodynamic driving force and slightly lower kinetic barrier.

1. Introduction

The study of new reactions that involve C−C bond activation constitutes a very active field of research in organometallic chemistry.[1] A limited number of C−C bond oxidative addition reactions in alkyl and aryl cyanides by transition metals have been reported.[2] These activated compounds are involved in reactions such as the selective functionalization of organic nitriles[3,4] and the cycloaddition of nitriles.[5] The C−C bond cleavage of acetonitrile has been achieved by the photolysis of the *ansa*-molybdenocene, $[Me_2Si(C_5Me_4)_2]$-MoH_2,[6] from the reaction of a cationic Rh(III) silyl complex, $[Cp^*(PMe_3)Rh(SiPh_3)(CH_2Cl_2)]BAr_4'$,[7] and with the photoreaction of a silyl iron complex $Cp(CO)_2Fe(SiMe_3)$.[8] Theoretical studies on the trimethylsilyl-assisted C−C bond cleavage of TMS-bound acetonitrile were reported by Nakazawa.[8a] Catalytic nitrile-group transfer from acetonitrile to aryl halides by palladium bisphosphine complexes in the presence of zinc metal powder to give the ArCN compounds has been reported by Luo.[9] Despite these reports, there is only a limited understanding of how C−C bond cleavage occurs in nitriles.

[†] University of Rochester.
[‡] Universidad Nacional Autónoma de México.

(1) For reviews of C−C bond activation by organometallic complexes, see: (a) Murakami, M.; Ito, Y. In *Topics in Organometallic Chemistry*; Murai, S., Ed.; Springer-Verlag: New York, 1999; pp 97−129. (b) Rybtchinski, B.; Milstein, M. *Angew. Chem., Int. Ed.* **1999**, *38*, 870−883. (c) Perthuisot, C.; Edelbach, B. L.; Zubris, D. L.; Simhai, N.; Iverson, C. N.; Muller, C.; Satoh, T.; Jones, W. D. *J. Mol. Catal. A* **2002**, *189*, 157−168. (d) Jun, C.-H. *Chem. Soc. Rev.* **2004**, *33*, 610.

(2) (a) Abla, M.; Yamamoto, T. *J. Organomet. Chem.* **1997**, *532*, 267. (b) Favero, G.; Movillo, A.; Turco, A. *J. Organomet. Chem.* **1983**, *241*, 251. (c) Morvillo, A.; Turco, A. *J. Organomet. Chem.* **1981**, *208*, 103. (d) Parshall, G. W. *J. Am. Chem. Soc.* **1974**, *96*, 2360. (e) Gerlach, D. H.; Kane, A. R.; Parshall, G. W.; Jesson, J. P.; Muetterties, E. L. *J. Am. Chem. Soc.* **1971**, *93*, 3543. (f) Burmeister, J. L.; Edwards, L. M. *J. Chem. Soc. A* **1971**, 1663. (g) Garcia, J. J.; Jones, W. D. *Organometallics* **2000**, *19*, 5544. (h) Garcia, J. J.; Brunkan, N. M.; Jones, W. D. *J. Am. Chem. Soc.* **2002**, *124*, 9547. (i) Liu, Q.-X.; Xu, F.-B.; Li, Q.-S.; Song, H.-B.; Zhang, Z.-Z. *Organometallics* **2004**, *23*, 610. (j) Ozawa, F.; Iri, K.; Yamamoto, A. *Chem. Lett.* **1982**, 1707. (k) Adam, R.; Villiers, C.; Ephritikhine, M.; Lance, M.; Nierlich, M.; Vigner, J. *J. Organomet. Chem.* **1993**, *445*, 99. (l) Marlin, D. S.; Olmstead, M. M.; Mascharak, P. K. *Angew. Chem., Int. Ed.* **2001**, *40*, 4752. (m) Lu, T.; Zhuang, X.; Li, Y.; Chen, S. *J. Am. Chem. Soc.* **2004**, *126*, 4760.

(3) (a) Miller, J. A. *Tetrahedron Lett.* **2001**, *42*, 6991. (b) Miller, J. A.; Dankwardt, J. W. *Tetrahedron Lett.* **2003**, *44*, 1907. (c) Miller, J. A.; Dankwardt, J. W.; Penney, J. M. *Synthesis* **2003**, *11*, 1643. (d) Penney, J. M.; Miller, J. A. *Tetrahedron Lett.* **2004**, *45*, 4989. (e) Crestani, M. G.; Arevalo, A.; Garcia, J. J. *Adv. Synth Catal.* **2006**, *348*, 732. (f) Crisostomo, C.; Crestani, M. G.; Garcia, J. J. *J. Mol. Catal.* **2007**, *266*, 139. (g) Nakao, Y.; Oda, S.; Hiyama, T. *J. Am. Chem. Soc.* **2004**, *126*, 13904−13905. (h) Nakao, Y.; Hiyama, T. *Jpn. Kokai Tokkyo Koho* **2006**, 19pp. (i) Nakao, Y.; Yada, A.; Satoh, J.; Ebata, S.; Oda, S.; Hiyama, T. *Chem. Lett.* **2006**, *35*, 790. (j) Nakao, Y.; Oda, S.; Yada, A.; Hiyama, T. *Tetrahedron* **2006**, *62*, 7567. (k) Nakao, Y.; Kanyiva, K. S.; Oda, S.; Hiyama, T. *J. Am. Chem. Soc.* **2006**, *128*, 8146. (l) Nakao, Y.; Yada, A.; Ebata, S.; Hiyama, T. *J. Am. Chem. Soc.* **2007**, *129*, 2428.

(4) Tobisu, M.; Kita, Y.; Chatani, N. *J. Am. Chem. Soc.* **2006**, *128*, 8152.

(5) (a) Bruce, M. I.; Skelton, B. W.; White, A. H.; Zaitseva, N. N. *J. Chem. Soc., Dalton Trans.* **2001**, 3627. (b) Bruce, M. I.; Skelton, B. W.; White, A. H.; Zaitseva, N. N. *Inorg. Chem. Commun.* **2001**, *4*, 617. (c) Bruce, M. I.; Skelton, B. W.; White, A. H.; Zaitseva, N. N. *J. Organomet. Chem.* **2002**, *650*, 141. (d) Chan, K. S.; Li, X. Z.; Fung, C. W.; Zhang, L. *Organometallics* **2007**, *26*, 20.

(6) Churchill, D.; Shin, J. H.; Hascall, T.; Hahn, J. M.; Bridgewater, B. M.; Parkin, G. *Organometallics* **1999**, *18*, 2403.

(7) (a) Taw, F. L.; White, P. S.; Bergman, R. G.; Brookhart, M. *J. Am. Chem. Soc.* **2002**, *124*, 4192. (b) Taw, F. L.; Mueller, A. H.; Bergman, R. G.; Brookhart, M. *J. Am. Chem. Soc.* **2003**, *125*, 9808.

(8) (a) Nakazawa, H.; Kawasaki, T.; Miyoshi, K.; Suresh, C. H.; Koga, N. *Organometallics* **2004**, *23*, 117. (b) Nakazawa, H.; Kamata, K.; Itazaki, M. *Chem. Commun.* **2005**, 4004. (c) Itazaki, M.; Nakazawa, H. *Chem. Lett.* **2005**, *34*, 1054.

(9) Luo, F.-H.; Chu, C.-I.; Cheng, C.-H. *Organometallics* **1998**, *17*, 1025.

10.1021/ja0707153 CCC: $37.00

Previously, we have reported that the reaction of acetonitrile with $[Ni(dippe)H]_2$ (**1**) favors the initial η^2 coordination of the nitrile to nickel(0) and gives only the C−CN bond activation product under both thermal and photochemical conditions (eq 1).[10] Although the reaction of **1** with allyl cyanide provides

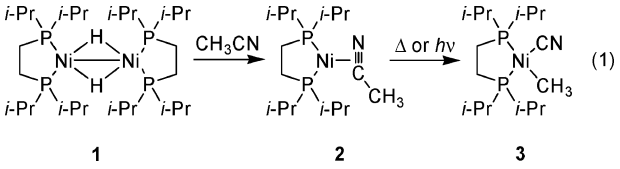

evidence for C−H bond activation,[11] no C−H oxidative addition product was observed in the reaction with acetonitrile. This might be due to the instability of the C−H oxidative addition product at the reaction temperature or the more favorable C−CN bond activation pathway. In this paper, the stability of the C−H oxidative addition product was examined by its independent synthesis from $LiBEt_3H$ reduction of $[Ni(dippe)(CH_2CN)Cl]$ (**4-Cl**). We also conducted DFT calculations incorporating solvent on [Ni(dmpe)] (dmpe = bis(dimethyl-phosphino)ethane), as a model for the [Ni(dippe)] fragment, to examine the energetics and reaction pathways leading to the C−CN and C−H oxidative addition products and to identify the factors that favor C−CN activation over C−H activation. To the best of our knowledge, this is the first theoretical study on the bond activation of acetonitrile which demonstrates the critical importance of taking into account the effect of solvation.

2. Results and Discussion

2.1. Synthesis of [Ni(dippe)(CH_2CN)Cl] (4-Cl). The reaction of **1** with chloroacetonitrile in benzene at room temperature yields **4-Cl** quantitatively (eq 2). The $^{31}P\{^1H\}$ NMR spectrum

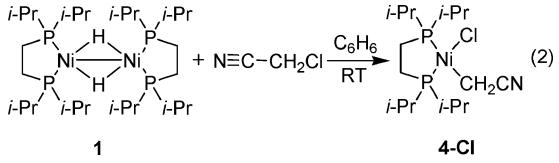

of **4-Cl** shows two doublets, indicating the presence of two chemically inequivalent phosphines, at δ 77.41 and 81.11 ($^2J_{P-P}$ = 29 Hz). These coupling constants are typical for asymmetric nickel(II) bisphosphine compounds. The ^1H NMR spectrum shows four doublets of doublets for the methyl resonances of the isopropyl groups, two multiplets for their methyne protons, and one multiplet at δ 1.29 for the methylene protons of the nitrile. The nitrile carbon has a similar chemical shift (δ 115.9) in the ^{13}C NMR spectrum to that of the free chloroacetonitrile (δ 117.3). The structure of **4-Cl** was also confirmed by an X-ray structure determination, as depicted in Figure 1; selected bond lengths and angles are given in the figure caption.

2.2. Reduction of [Ni(dippe)(CH_2CN)Cl] (4-Cl) with $LiHBEt_3$. In the low-temperature reduction of **4-Cl** with $LiHBEt_3$, a hydride peak was observed in the ^1H NMR spectrum only at temperatures below −40 °C. This hydride peak, which appears

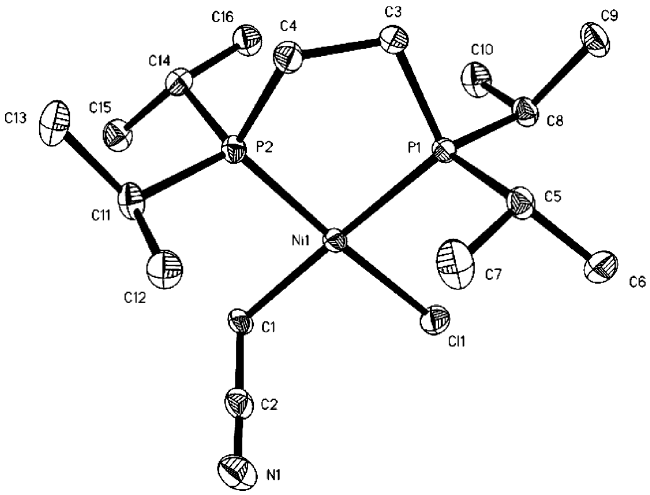

Figure 1. ORTEP drawing of **4-Cl**. Ellipsoids are shown at the 50% probablility level. Hydrogen atoms are omitted for clarity. Selected bond lengths (Å): Ni(1)−C(1), 2.0135(14); Ni(1)−P(1), 2.2010(5); Ni(1)−P(2), 2.1341(5); Ni(1)−Cl(1), 2.2165(5); C(1)−C(2), 1.445(2); C(2)−N(1), 1.153-(2). Selected angles (deg): P(1)−Ni(1)−P(2), 88.34(2); P(1)−Ni(1)−Cl-(1), 90.04(2); P(2)−Ni(1)−C(1), 91.26(5); C(1)−Ni(1)−Cl(1), 90.60(5); Ni(1)−C(1)−C(2), 107.00(10).

as a doublet of doublets at δ −10.1 ($^2J_{H-P}$ = 80, 160 Hz), was assigned to $[Ni(dippe)(CH_2CN)H]$ (**4**) (eq 3).

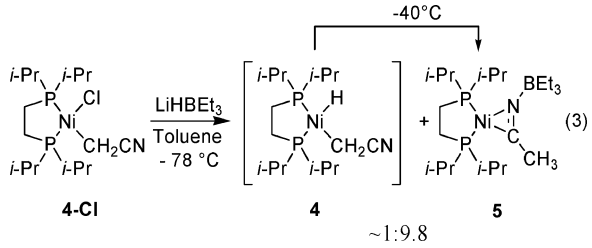

The $^{31}P\{^1H\}$ NMR spectrum showed two doublets at δ 91.2 and 70.1 ($^2J_{P-P}$ = 5 Hz) for the two chemically inequivalent phosphines of **4**. As the temperature was increased above −40 °C, these phosphorus resonances disappeared, as did the hydride resonance in the ^1H NMR spectrum. At all temperatures, the $^{31}P\{^1H\}$ NMR spectrum also showed the presence of another nickel complex with a P−P coupling constant of 47 Hz, an unusually high value for nickel(II) compounds. The ratio of **4** to this nickel(II) complex was approximately 1:9.8 at −60 °C. This unknown compound was assigned as the BEt_3 adduct of the η^2-nitrile complex, $[Ni(dippe)(\eta^2\text{-}CH_3CN{-}BEt_3)]$ (**5**). Proof for the proposed structure was obtained by independent synthesis.

2.3. Synthesis of [Ni(dippe)($CH_3CN{-}BEt_3$)] (5). The room-temperature reaction of **1** with acetonitrile in the presence of BEt_3 in hexanes yields **5** quantitatively (eq 4). The $^{31}P\{^1H\}$

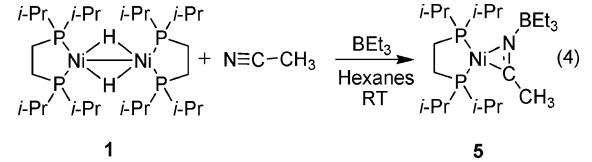

NMR spectrum shows two doublets, characteristic of two chemically inequivalent phosphines with resonances at δ 79.43 and 63.07 ($^2J_{P-P}$ = 47 Hz). These coupling constants are typical for similar low-valent nickel compounds containing Lewis acid

(10) Garcia, J. J.; Arevalo, A.; Brunkan, N. M.; Jones, W. D. *Organometallics* **2004**, *23*, 3997−4002.
(11) Brunkan, N. M.; Brestensky, D. M.; Jones, W. D. *J. Am. Chem. Soc.* **2004**, *126*, 3627−3641.

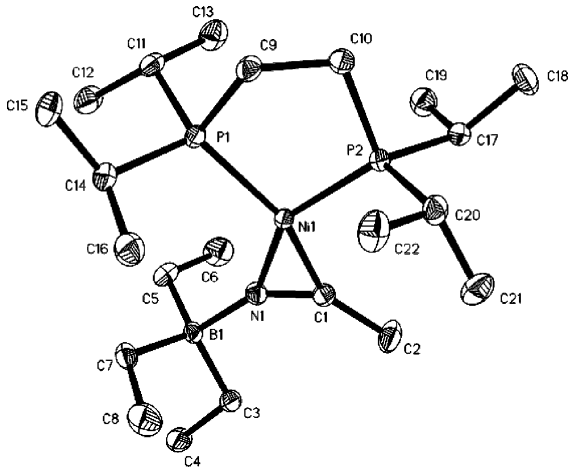

Figure 2. ORTEP drawing of **5**. Ellipsoids are shown at the 50% probablility level. Hydrogen atoms are omitted for clarity. Selected bond lengths (Å): Ni(1)−C(1), 1.8438(18); Ni(1)−N(1), 1.9021(15); Ni(1)−P(1), 2.1983(6); Ni(1)−P(2), 2.1377(6); C(1)−C(2), 1.494(3); C(1)−N(1), 1.234(2); B(1)−N(1), 1.610(2). Selected angles (deg): P(1)−Ni(1)−P(2), 91.43(2); P(1)−Ni(1)−N(1), 121.59(5); P(2)−Ni(1)−C(1), 108.53(6); C(1)−Ni(1)−N(1), 38.42(7); N(1)−C(1)−C(2), 137.99(18).

adducts of η^2-nitriles.[2g,h] The ^{1}H NMR spectrum shows a doublet at δ 2.472 ($^4J_{H-P}$ = 4.8 Hz) for the methyl group of the acetonitrile. The ^{13}C NMR spectrum shows the resonance of the nitrile carbon at δ 163.6 (dd, $^2J_{C-P}$ = 42, 7 Hz) and the resonance of the acetonitrile methyl group at δ 16.8 (dd, $^2J_{C-P}$ = 13, 10 Hz). This compound is assigned as **5** in analogy to [Ni(dippe)(η^2-CH_3CNBPh_3)].[9] The structure of **5** was also confirmed by an X-ray structure determination, as depicted in Figure 2; selected bond lengths and angles are given in the figure caption. The C−N bond lengthens from 1.153 Å in acetonitrile[12] to 1.234(2) Å in **5** (1.236(4) Å in BPh_3 analogue), and the N−C−CH_3 angle deviates from linearity to an angle of 137.9(2)° (136.8(3)° in BPh_3 analogue).

Complex **5** is thermally very stable. Even after heating a solution of **5** at 100 °C for 2 days, no C−CN bond cleavage product was observed. However, upon irradiation with UV light for 2 h, half of **5** was converted to the BEt_3 adduct of the C−CN bond cleavage product, [Ni(dippe)(CH_3)(CN−BEt_3)] (**6**). **6** displays two doublets in the ^{31}P NMR spectrum at δ 77.72 and 78.86 (J_{P-P} = 17 Hz), consistent with a Ni(II) species. The complex can be independently prepared by addition of BEt_3 to **3**, and its ^{31}P NMR resonances are shifted downfield by about 1 ppm from those of **3**. Based on the observed Lewis acid inhibition of the thermal C−CN bond cleavage, a Lewis base, NEt_3, was added to the $LiHBEt_3$ reduction of **4-Cl**. The ^{31}P NMR spectrum below −40 °C showed that a larger amount of **4** was formed than when no base was used. The new ratio of **4** to **5** was approximately 1:1.2 at −60 °C.

2.4. Photochemical Reaction of [Ni(dippe)H]$_2$ (1) with Acetonitrile at Low Temperature. The C−H oxidative addition product, **4**, was not observed from the thermal and photochemical reactions of **1** with CH_3CN due to its instability at temperatures above −40 °C. To test whether the C−H bond activation pathway competes with the C−CN bond activation pathway, a mixture of **1** and CH_3CN was irradiated with UV light at −65 °C. However, even under these conditions, only the C−CN bond cleavage product Ni(dippe)(CH_3)(CN) (**3**) was observed, indicating that the C−CN bond activation pathway is kinetically more facile than the C−H bond activation pathway. The lack of C−H activation of acetonitrile by **1** is particularly surprising in that many such reactions are known to give stable C−H oxidative addition products.[13] For example, the fragment [Tp′RhL] where L = CNneopentyl reacts with acetonitrile to give exclusively Tp′LRh(H)(CH_2CN),[14] and [Fe(dmpe)$_2$] reacts to give Fe(dmpe)$_2$(H)(CH_2CN).[15] In neither of these cases is either η^2-coordination or C−CN activation observed.

2.5. Computational Results. Based on the observations that the reaction of **1** with acetonitrile gave only the C−CN bond activation product and that **4** is not stable at temperatures above −40 °C, a computational study was undertaken to examine the energetics and reaction pathways leading to the C−CN and C−H oxidative addition products and to identify the factors that favor C−CN activation over C−H activation. The reaction of the [Ni(dmpe)] fragment with acetonitrile was used as a model. Initially, local minima for the η^2-nitrile, Ni(dmpe)(η^2-CH_3CN) (**S1**), and the C−CN oxidative addition product, Ni(dmpe)(CH_3)(CN) (**S5**), were found in gas-phase calculations. The relative energies of these structures, however, contradicted the experimental observations in that **S5** was found to lie 4.1 kcal mol^{-1} higher in energy than **S1**. This difference was attributed to the high polarity of the C−CN oxidative addition product (dipole moment = 14.3 Debye) and the lack of inclusion of solvation effects. Therefore, solvent effects on the geometries and relative stabilities of all structures were taken into consideration in all further calculations in terms of the polarizable continuum model (PCM).[16] Inclusion of solvation using this model shows **S5** to now lie 2.1 kcal mol^{-1} below **S1**. The optimized structural parameters and relative energies of all stable species and transition states found in this study are summarized in Table 1, Scheme 1, and Figure 3. The gas-phase optimizations gave very similar structures for all species (see Table SI-2).

One unexpected aspect of this study was the location of a stable, high energy (+29.8 kcal mol^{-1} relative to **S1**) species, **S3**, which can be described as an η^3-H,C,C-acetonitrile complex containing an agostic C−H interaction with the metal center. The hydrogen is 1.84 Å from nickel, and the C−H bond is lengthened to 1.13 Å. The H−C−C−N atoms of the acetonitrile and the nickel lie in a plane that is at a 90° angle to the P−Ni−P plane, and the C−C−N bond is bent to 159.1°. As described later, this stable species lies in a shallow well on a relatively flat surface connecting to transition states leading to products **S1**, **S5**, and **S7**.

Of the optimized structures summarized in Scheme 1, only the dippe analogues of the η^2 coordinated nitrile (**S1** ≈ **2**) and the C−CN oxidative addition product (**S5** ≈ **3**) are stable enough to be isolated. Of the two, only **3** has X-ray crystallographic data available; however, the distances obtained from this structure are inaccurate due to the disorder between the methyl and cyanide groups.[9] Nevertheless the optimized structures of

(12) Kratochwill, A.; Weidner, J. U.; Zimmermann, H. *Ber. Dtsch. Bunsen-Ges.* **1973**, *77*, 408.

(13) Heeres, H. J.; Meetsma, A.; Teuben, J. H. *Angew. Chem., Int. Ed. Engl.* **1990**, *29*, 420.

(14) Vetter, A. J.; Rieth, R. R.; Jones, W. D. *Proc. Natl. Acad. Sci. U.S.A.* **2007**, in press.

(15) Ittel, S. D.; Tolman, C. A.; English, A. D.; Jesson, J. P. *J. Am. Chem. Soc.* **1978**, *100*, 7577.

(16) This model treats the solvent as a sphere of the appropriate size that is rolled over the surface of the molecule, with the dipole of the solvent interacting optimally to stabilize the molecule. See: Miertus, S.; Scrocco, E.; Tomasi, J. *Chem. Phys.* **1981**, *55*, 117.

Table 1. Optimized Structural Parameters (Å, deg) and Relative Free Energies (ΔG, kcal/mol) of Stationary Points on the [Ni(dmpe)] + CH_3CN Potential Energy Surface (Atom Numbering Is as Shown in Figure 2)

	Ni–C1	Ni–C2	C1–C2	Ni–H[a]	Ni–N	N–C2	C–H	N–C1–C2	Ni–C2–N	ΔG[b]
S1	3.22	1.86	1.49	3.82	1.92	1.23	1.09	138.5	73.8	−33.19
TS2	2.50	1.94	1.49	2.16	2.57	1.19	1.11	158.8	108.3	−2.53
S3	2.27	1.96	1.49	1.84	2.74	1.18	1.13	159.1	119.6	−3.38
TS4	2.12	1.82	1.68	2.00	2.92	1.19	1.11	133.3	150.0	−1.14
S5	1.96	1.88	2.73	2.51	3.05	1.17	1.10	136.6	177.4	−35.28
TS6	2.11	2.68	1.45	1.51	3.54	1.17	1.32	177.9	129.2	0.11
S7	1.99	2.74	1.44	1.48	3.64	1.17	2.44	177.6	133.1	−20.03

[a] Shortest Ni−H distance. [b]Total free energies in solution.

Scheme 1. Optimized Structures (Distances in Å, Angles in deg) of Stationary Points on the [Ni(dmpe)] + CH_3CN Potential Energy Surface

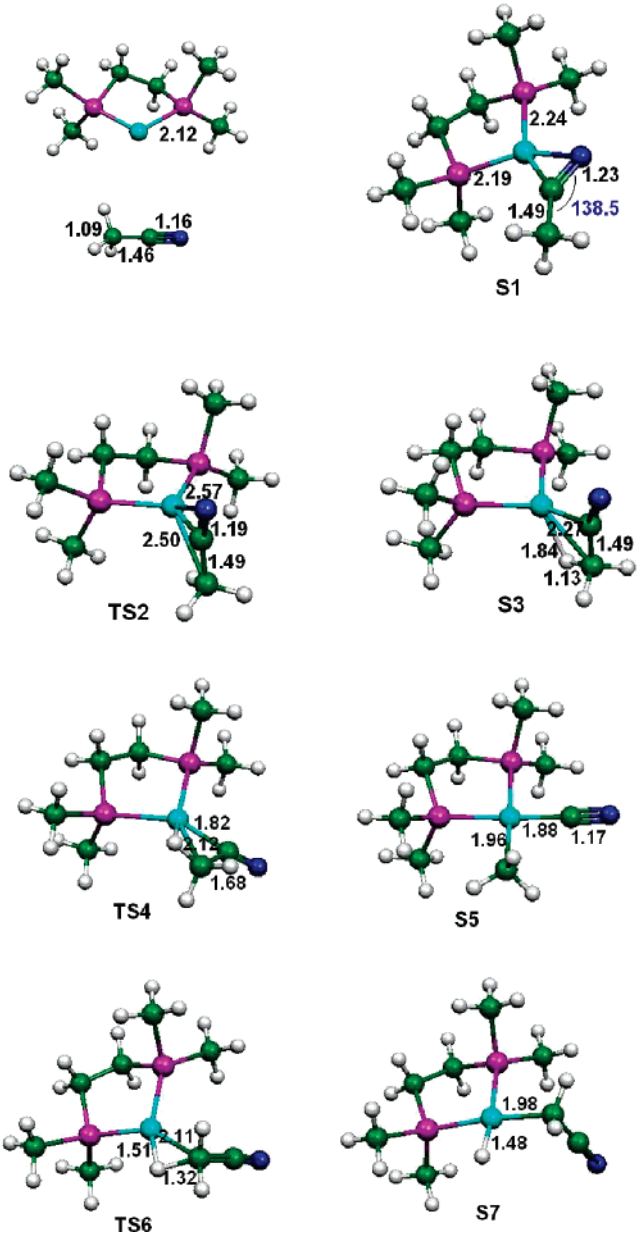

S1 and **S5** are highly consistent with the crystallographic data available for other nickel nitrile complexes.[2g,h] In **S1**, the coordinated C−N bond is longer than that in free acetonitrile (1.23 vs 1.16 Å), and the nitrile group deviates from linearity (C−C−N angle is 138.5° vs 180°). The Ni−P bonds are

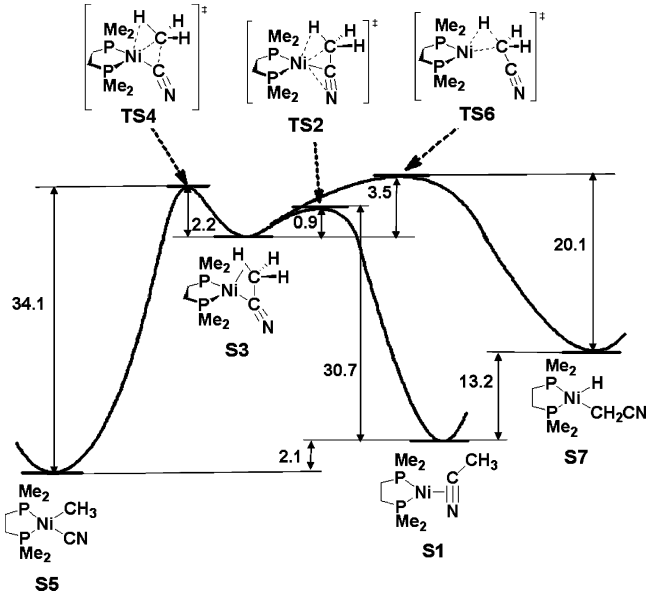

Figure 3. Energetics of C−C and C−H bond activation of acetonitrile by [Ni(dmpe)] (free energies in kcal mol^{-1} at 298 K) relative to the total energies of fragments ([Ni(dmpe)] and CH_3CN).

lengthened relative to [Ni(dmpe)], due to the trans influence of the nitrile ligand.

The optimized structures of the C−CN and C−H bond activation products (**S5** and **S7**) have the expected square-planar geometry around the metal center. The calculated total free energies in solution indicate that **S5** is 2.1 kcal mol^{-1} more stable than the η^2-coordinated nitrile and 15.3 kcal mol^{-1} more stable than **S7**. Consequently, the thermodynamic instability of the C−H activation product **4** observed experimentally is also borne out in the calculations.

As mentioned above, an unstable η^3-agostic-CH intermediate lies at the center of the reactivity in this system. This species is only slightly preferred over the [Ni(dmpe)] fragment plus acetonitrile, which explains why the thermal reactions lead to decomposition unless they are carried out in the presence of excess CH_3CN. The lowest energy transition state, **TS2**, connects the η^2-coordinated nitrile **S1** to the η^3-coordinated intermediate **S3** as confirmed by an intrinsic reaction coordinate calculation (IRC) starting from **TS2**, which is 30.7 kcal mol^{-1} higher in energy than the η^2-nitrile. The nitrile in **TS2** coordinates to the nickel center through the nitrile carbon (Ni−CN = 1.94 Å) and, more weakly, through its nitrogen and methyl carbon atoms (Ni−N = 2.57 Å, Ni−C = 2.50 Å). The plane defined by these three atoms, C−C−N, is perpendicular to the P−Ni−P plane. **S3** corresponds to a weakly bound σ C−C bond with agostic C−H interaction and lies on a shallow local minimum only 0.9 kcal mol^{-1} lower in energy than **TS2**.

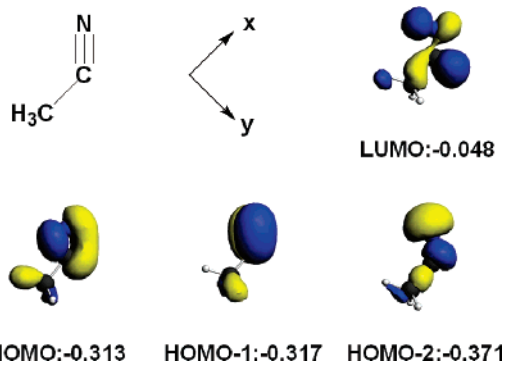

Figure 4. Two highest occupied and the lowest unoccupied MOs for bent MeCN, their corresponding energies (eV), and the chosen coordinate system. The *x* and *y* axes lie in the plane of the page.

Motion along the reaction coordinate at **TS2** looks like a rocking motion, in which the agostic C−H or η^2-nitrile alternately approach the metal from above or below the NiP_2 plane.

TS4, the transition state leading to the C−CN bond cleavage product **S5**, was located 2.2 kcal mol^{-1} higher in energy than **S3**, while that of **TS6**, the transition state leading to the C−H bond cleavage product **S7**, lies 3.5 kcal mol^{-1} higher. In **TS4**, the C−CN bond is 0.19 Å longer than that in **S1**, and the C−C−N angle is 133.3°, similar to that in **S1**. However, the nitrogen is now distant from the metal with a Ni−C−N angle of 150.0°. The methyl carbon moves to 2.12 Å from nickel, halfway to its target value of 1.96 Å in **S5**. The cyano carbon is only 1.82 Å from nickel which is 0.06 Å *closer* than that in the product **S5**. Also, the C−C−N plane has now rotated to an angle of 38° relative to the P−Ni−P plane. The C−C bond is lengthened to 1.68 Å. Consequently, the C−C bond cleavage transition state can be viewed as well-progressed toward the nickel(II) square planar product.

In **TS6** the C−H bond length is 0.23 Å longer than that in **S1**. The hydrogen is only 1.51 Å from nickel, and the carbon is 2.11 Å from nickel, only 0.13 Å longer than its target value in **S7**. The Ni−C−H plane is twisted only 4.2° relative to the P−Ni−P plane. Even more so than in the transition state for C−C bond cleavage, **TS6** is well along the way to the product **S7**. The higher kinetic barrier and the absence of a thermodynamic driving force for the C−H bond activation are fully consistent with the experimental observation that only the C−C bond activation product is formed.

2.6. MO Analysis. The electronic structures of **S1**−**TS4** were analyzed with the help of the fragment molecular orbital approach considering symmetry and energy requirements for the possible donation and back-donation interactions.[17] The molecular orbitals were calculated for the bent acetonitrile, as this is the geometry it adopts upon coordination to the nickel fragment. Both the HOMO (highest occupied molecular orbital) and the HOMO-1 are mainly nitrile π bonding orbitals, whereas the LUMO (lowest unoccupied molecular orbital) is the nitrile π^* antibonding orbital (Figure 4). The LUMO is in the same plane with the HOMO, and they are in the plane of the bent acetonitrile molecule; the HOMO−1 is perpendicular to this plane. The HOMO−2 is mainly the C−C and C−N σ bonding orbital, which consists of in-plane p orbital interactions on the two carbons and the nitrogen, and also encompasses the nitrogen lone pair.

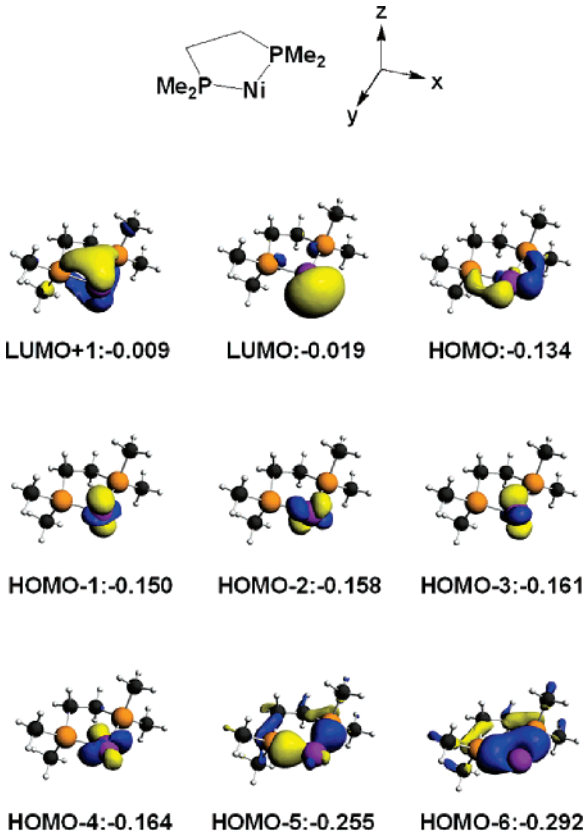

Figure 5. Two lowest unoccupied and eleven highest occupied MOs for [Ni(dmpe)] fragment, their corresponding energies (eV), and the chosen coordinate system. The *x* and *y* axes are in a plane, and the z axis is perpendicular to the plane.

The electron density of the two lowest unoccupied and the five highest occupied molecular orbitals of the [Ni(dmpe)] fragment are localized mainly on the nickel atom. The LUMO+1 is mainly Ni p_z orbital (see Figure 5 for the definition of the coordinate system), which has a π orbital symmetry perpendicular to the ligand ring system, while the LUMO is mainly Ni sp hybrid orbital directed toward the incoming acetonitrile ligand and it is in the plane of the ligand ring system. The HOMO is predominantly the $3d_{x^2-y^2}$ orbital and the next four highest occupied molecular orbitals are the nonbonding $3d_{z^2}$ and combinations of the $3d_{xy}$, $3d_{xz}$, and $3d_{yz}$ orbitals of the nickel atom. The HOMO−5 and HOMO−6 are mainly the Ni−P σ bonding orbitals with some contribution from the nickel $3d_{x^2-y^2}$ and 4s orbitals, respectively. The remaining highest occupied molecular orbitals consist mainly of the backbone bonding interactions.

The most important bonding interactions in **S1** result from the back-donation of electron density from the HOMO of the metal fragment into the LUMO of the acetonitrile (Figure 6). ADF fragment analysis shows that the HOMO of the acetonitrile mixes with the HOMO−6 of the metal fragment to give a bonding and an antibonding combination, which are both bonding between the acetonitrile ligand and the metal center. (See Supporting Information for fragment interaction diagram.) The antibonding combination is stabilized by mixing with the LUMO of the metal fragment. HOMO−1 of the acetonitrile

(17) Velde, G.; Bickelhaupt, F.; van Gisbergen, S.; Guerra, C.; Baerends, E.; Snijders, J.; Ziegler, T. *J. Comput. Chem.* **2001**, *22*, 931. Guerra, C.; Snijders, J.; te Velde, G.; Baerends, E. *Theor. Chem. Acc.* **1998**, *99*, 391. ADF2006.01, SCM, Theoretical Chemistry; Vrije Universiteit: Amsterdam, The Netherlands, http://www.scm.com.

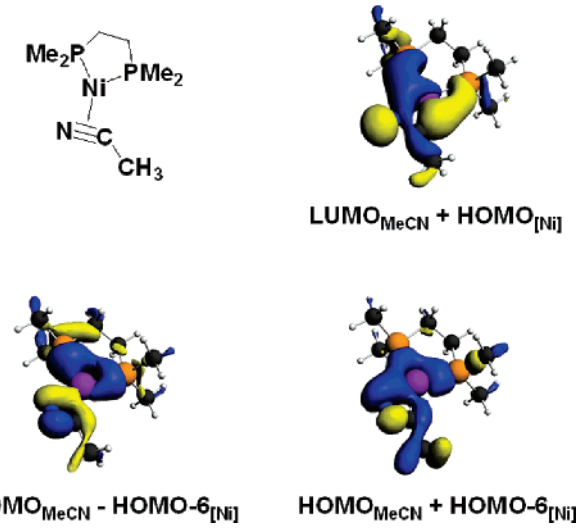

Figure 6. Three most important bonding interactions between the metal fragment and the acetonitrile ligand in **S1**.

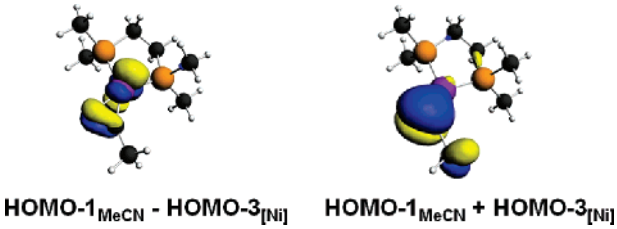

Figure 7. π bonding and π^* antibonding interactions between the metal fragment and the acetonitrile ligand in **S1**.

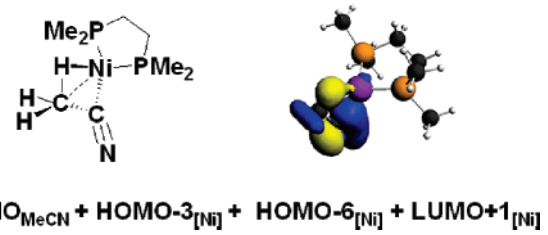

Figure 8. MO showing the agostic C−H interaction with nickel in **S3**.

has the correct symmetry to mix with the HOMO−3 of the metal fragment. The resulting bonding and antibonding combinations are shown in Figure 7. (See Supporting Information for fragment interaction diagram.) The bonding combination is further stabilized due to the mixing with the LUMO+1 of the metal fragment. The square planar geometry for **S1** is more in accord with a d^8 configuration for nickel rather than d^{10} as a result of extensive π backbonding to the LUMO of the acetonitrile, which is the π^* orbital of the bent acetonitrile ligand.

The nickel nitrile bonding interactions and C−H agostic interaction to nickel in **S3** result from the mixing of the HOMO of the acetonitrile with the HOMO−3, HOMO−6, and the LUMO+1 of the metal fragment (Figure 8). Although **S3** is stabilized by this weak agostic interaction, the absence of effective metal to ligand backbonding, due to the C−C−N plane being perpendicular to the P−Ni−P plane, leads to it being only 3.4 kcal mol more stable than the individual fragments. The MOs of **TS2** are very similar to those of **S3** since **TS2** is a late transition state; i.e., the energy difference between **TS2** and **S3** is very small.

The bonding interactions in **TS4** are crucial to understand the reactivity of the nickel fragment toward acetonitrile, since

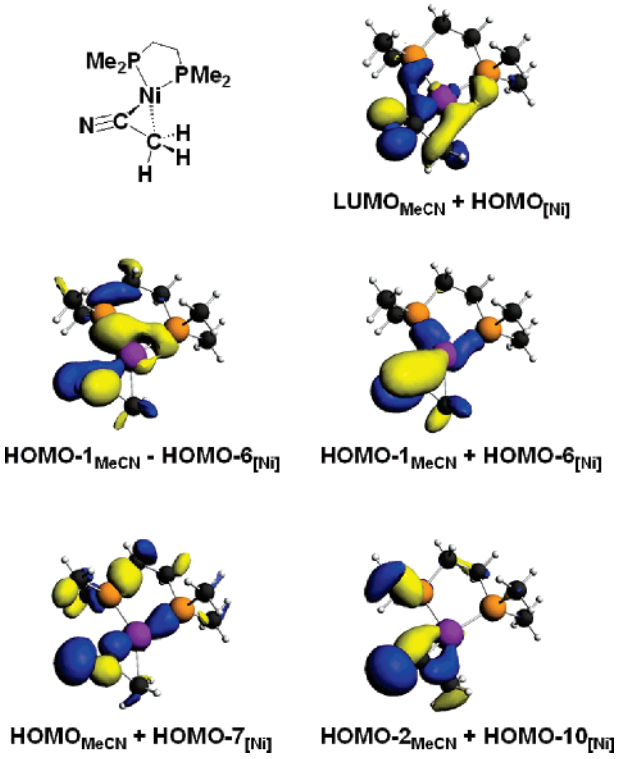

Figure 9. MOs showing the formation of the Ni−CN σ bond, π bond, and the Ni−CH_3 σ bond and the cleavage of the C−CN bond in **TS4**.

it leads to the formation of the C−CN oxidative addition product, the only observed product in this reaction. The back-donation from the metal fragment HOMO ($d_{x^2-y^2}$) to the acetonitrile LUMO results in the formation of the Ni−CH_3 σ bonding interaction (Figure 9). This MO is also significant in that it is σ antibonding in character with respect to the C−CN bond as well as the agostic C−H interaction. Thus it not only leads to bond formation, but it also leads to the cleavage of the C−CN bond. The mixing of the HOMO and the HOMO−1 of acetonitrile with the HOMO−7 and the HOMO−6 of the metal fragment results in the formation of Ni−CN σ bonding and π bonding interactions, respectively. The other important molecular orbital of **TS4** results from the mixing of the HOMO−2 of the acetonitrile with the HOMO−10 of the nickel fragment and leads to the σ bonding interaction between the metal center and the methyl carbon. (See Supporting Information for fragment interaction diagram.) The dihedral angle between the P−Ni−P plane and the C−C bond being cleaved is 38°. **TS4** can therefore be viewed as halfway between a d^{10} nickel(0) tetrahedral complex of the acetonitrile and d^8 nickel(II) square planar methyl cyano product.

3. Conclusions

The reaction of **1** with acetonitrile leads only to the C−CN bond activation product due to both the kinetic and thermodynamic preference of C−CN bond activation over C−H bond activation. The C−H activation product was only observed at temperatures below −40 °C in the reduction of **2** with $LiHBEt_3$. Due to the polarity of the C−CN bond cleavage products, solvent effects were taken into consideration in all DFT calculations in terms of PCM in order to achieve good agreement with experiment. Three transition states were located on the potential energy surface of the reaction. The first transition

state connects the η^2-nitrile with a weakly bound η^3-nitrile intermediate via migration of the metal from the C−N bond to the C−C bond, while the other two transition states lead to the respective bond activation products. The transition states indicate that substantial bond making occurs prior to C−CN bond rupture.

4. Experimental Section

4.1. General Procedures. All reactions were carried out using standard Schlenk and glovebox techniques, under nitrogen. Solvents, including deuterated solvents (Cambridge Isotope Laboratories), were dried and distilled before use from sodium/benzophenone ketyl. All other chemicals, filter aids, and chromatographic materials were reagent grade and were used as received. ^{1}H, ^{13}C, and ^{31}P NMR spectra were determined on an AVANCE400 spectrometer in benzene-d_6 or THF-d_8 unless otherwise stated; chemical shifts (δ) are relative to the deuterated solvent residual protons, and ^{31}P NMR spectra are relative to external reference 85% H_3PO_4. Photolysis experiments were done using an Oriel 200 W Hg/Xe lamp. Elemental analyses were carried out by Desert Analytics, Tuscon, AZ. The synthesis of [Ni(dippe)H]$_2$ was carried out using the previously reported procedure.[18] Acetonitrile and chloroacetonitrile were purchased from Aldrich and distilled before use. All complexes were purified by crystallization.

4.2. Computational Details. When available, known experimental structures for the complexes were used as the starting point for the calculations. To reduce computational time, the *i*-Pr groups were substituted by methyl groups. This model is assumed to have no steric outcome on the calculations but probably underestimates the donating ability of the P_2Ni fragment. The gas-phase structures were fully optimized in redundant internal coordinates,[19] with density-functional theory (DFT) and a wave function incorporating Becke's three-parameter hybrid functional (B3),[20] along with the Lee−Yang−Parr correlation functional (LYP).[21] (See Supporting Information for comparison with B3P86, P3PW91, BVWN, and the nontruncated model with the full dippe ligand.) All calculations were performed using the Gaussian03[22] package. The Ni and P atoms were represented with the effective core pseudopotentials of the Stuttgart group and the associated basis sets improved with a set of f-polarization functions for Ni (α = 3.130)[23] and a set of d-polarization functions for P (α = 0.387).[24] The remaining atoms (C, H, and N) were represented with 6-31G(d,p)[25] basis sets. The geometry optimizations were performed without any symmetry constraints, and the local minima and the transition states were checked by frequency calculations. For each transition-state structure, the intrinsic reaction coordinate (IRC) routes were calculated in both directions toward the corresponding minima. For some of the transition states, the IRC calculations failed to reach the energy minima on the potential energy surface; therefore, in those cases geometry optimizations were carried out as a continuation of the IRC path. Because of the polarity of the structures, the solvent effects on their relative stabilities were evaluated by calculating the free energies of solvation in terms of the polarizable continuum model (PCM).[16] The self-consistent reaction field (SCRF) calculations using the PCM-UA0 solvation model[26] were carried out for the gas-phase optimized structures as well as the PCM optimized structures. The dielectric constant in the PCM calculations was set to ϵ = 7.58 to simulate THF as the solvent medium used in the experimental study.[9] The energies discussed throughout the text are electronic energies with thermal corrections for ZPE. Gibbs free energies have been calculated at 298.15 K and 1 atm. The description of bonds between atoms as a linear combination of hybrids located on each partner of the bond was obtained from natural bonding orbital (NBO) calculations (see Supporting Information).[27] The Molden package was used to display the molecular orbitals and the electron densities.[28] The fragment analysis of the **S1**, **S3**, and **TS4** were examined using the ADF package of programs.[16]

4.3. Preparation of [Ni(dippe)(CH$_2$CN)Cl] (4-Cl). 4-Cl was prepared from the reaction of [Ni(dippe)H]$_2$ (**1**) (20 mg, 0.031 mmol) with chloroacetonitrile (4 μL, 0.063 mmol). **1** was dissolved in C_6D_6, and then chloroacetonitrile was added at room temperature. The color of the solution changed from dark red into light brown immediately. The NMR spectra demonstrated formation of **4-Cl** (yield 93%). To recrystallize complex **4-Cl**, C_6D_6 was removed under vacuum and the residue was dissolved in 0.6 mL toluene, using hexanes to help the crystallization process. The crystals of complex **4-Cl** were orange needles. Anal. Calcd for **4-Cl**, $C_{16}H_{34}ClNNiP_2$: C, 48.44; H, 8.65; N, 3.53. Found: C, 48.37; H, 8.36; N, 3.15. NMR spectra in benzene-d_6, ^{1}H: δ 0.837−0.889 (dd, $^2J_{P-H}$ = 2.8 Hz, $^2J_{H-H}$ = 5.6 Hz, 6H, CH_3), 0.928−0.978 (dd, $^2J_{P-H}$ = 2.8 Hz, $^2J_{H-H}$ = 5.3 Hz, 6H, CH_3), 1.054−1.113 (dd, $^2J_{H-H}$ = 6.6 Hz, $^2J_{P-H}$ = 2.9 Hz, 6H, CH_3), 1.333−1.390 (dd, $^2J_{H-H}$ = 6.4 Hz, $^2J_{P-H}$ = 2.8 Hz, 6H, CH_3), ∼1.021 (m, 2H, Ni−CH_2), 1.146−1.291 (m, 4H, CH_2), 1.704−1.794 (m, 2H, CH), 2.073−2.167 (m, 2H, CH); ^{31}P{^{1}H}: δ 77.41 (d, $^2J_{P-P}$ = 29 Hz), 81.11 (d, $^2J_{P-P}$ = 29 Hz); ^{13}C{^{1}H}: δ −8.5 (dd, Ni−CH_2), 18.229 (d, CH_3), 19.616 (dd, CH_3), 22.9 (m, CH_2), 24.8 (d, CH), 25.7 (d, CH), 115.9 (s, CN).

4.4. Preparation of [Ni(dippe)(CH$_2$CN)H] (4). 4.4.1. Reduction of 4-Cl by LiHBEt$_3$ (1.0 M in THF Solution). [Ni(dippe)H]$_2$ (21.6 mg, 0.033 mmol) was dissolved in toluene-d_8, and then chloroacetonitrile (4 μL, 0.062 mmol) was added at room temperature to give **4-Cl**. The reaction mixture was cooled to −78 °C in dry ice/acetone bath for 10 min, and then LiHBEt$_3$(0.06 mL, 0.06 mmol) was added slowly while the reaction mixture was still in the dry ice/acetone bath. ^{1}H and ^{31}P NMR spectra were recorded once every 10 °C as the reaction mixture was warmed from −60 °C to 40 °C in the NMR probe. NMR spectra in toluene-d_8, ^{1}H: δ −9.8 to −10.4 (dd, $^2J_{P-H}$ = 80 Hz, 1H, Ni−H hydride), 2.53 (d, J = 4.8 Hz, 3H, CH_3CN). ^{31}P{H}: major, δ 63.30 (d, $^2J_{P-P}$ = 45 Hz), 80.06 (d, $^2J_{P-P}$ = 45 Hz), minor, 71.62 and 92.25 (d, coupling constants are very small). **4:5** ∼1:9.8.

4.4.2. Reduction of 4-Cl by LiHBEt$_3$ (1.0 M in THF solution) in the Presence of NEt$_3$. [Ni(dippe)H]$_2$ (20.5 mg, 0.032 mmol) was dissolved in THF-d_8, and then chloroacetonitrile (3.8 μL, 0.059 mmol) was added at room temperature to get complex **4-Cl**. Excess NEt_3 (∼0.1 mL) was added. The mixture was cooled in dry ice/acetone bath for 10 min, followed by addition of 0.07 mL of LiHBEt$_3$ (0.06 mL, 0.06 mmol). Both ^{1}H and ^{31}P NMR spectra were taken once every 5 °C as the temperature slowly warmed from −60 °C to 25 °C. At −60 °C, NMR spectra in THF-d_8, ^{1}H: δ −9.9 to −10.5 (dd, $^2J_{P-H}$ = 80 Hz, 1H, Ni−H hydride). ^{31}P{^{1}H}: δ 61.87 (d, $^2J_{P-P}$ = 45 Hz), 78.87 (d, $^2J_{P-P}$ = 45 Hz), 91.2 (d, $^2J_{P-P}$ = 5 Hz), 70.1 (d, $^2J_{P-P}$ = 5 Hz). **4:5** ∼1:1.2

4.5. Preparation of [Ni(dippe)(CH$_3$CN−BEt$_3$)] (5). CH_3CN (1.6 μL, 0.031 mmol) and BEt_3 (0.031 mL, 0.031 mmol) were added successively to a hexanes solution (0.6 mL) of the nickel dimer [Ni(dippe)H]$_2$ (10 mg, 0.016 mmol) at room temperature. After mixing, the color of the reaction mixture changed from dark red to brown immediately. Then the solvent was evaporated slowly under a nitrogen flow overnight. Yield: 99% of pale yellow rodlike crystals. Anal. Calcd for **5**, $C_{22}H_{50}BNNiP_2$: C, 57.39; H, 10.95; N, 3.04. Found: C, 57.08;

(18) Vicic, D. A.; Jones, W. D. *J. Am. Chem. Soc.* **1997**, *119*, 10855.
(19) Peng, C.; Ayala, P. Y.; Schlegel, H. B.; Frisch, M. J. *J. Comput. Chem.* **1996**, *17*, 49.
(20) Becke, A. D. *J. Chem. Phys.* **1993**, *98*, 5648.
(21) Lee, C.; Yang, W.; Parr, R. G. *Phys. Rev. B* **1988**, *37*, 785.
(22) Frisch, M. J., et al. *Gaussian03*; Gaussian, Inc.: Wallingford, CT, 2004.
(23) Ehlers, A. W.; Bohme, M.; Dapprich, S.; Gobbi, A.; Hollwarth, A.; Jonas, V.; Kohler, K. F.; Stegmann, R.; Veldkamp, A.; Frenking, G. *Chem. Phys. Lett.* **1993**, *208*, 111.
(24) Hollwarth, A.; Bohme, M.; Dapprich, S.; Ehlers, A. W.; Gobbi, A.; Jonas, V.; Kohler, K. F.; Stegmann, R.; Veldkamp, A.; Frenking, G. *Chem. Phys. Lett.* **1993**, *208*, 237.
(25) Hehre, W. J.; Ditchfield, R.; Pople, J. A. *J. Chem. Phys.* **1972**, *56*, 2257.
(26) Barone, V.; Cossi, M.; Tomasi, J. *J. Chem. Phys.* **1997**, *107*, 3210.
(27) Reed, A. E.; Curtiss, L. A.; Weinhold, F. *Chem. Rev.* **1988**, *88*, 899.
(28) Schaftenaar, G.; Noordik, J. H. *J. Comput.-Aided Mol. Des.* **2000**, *14*, 123.

H, 11.05; N, 2.67. NMR spectra in benzene-d_6, ^{1}H: δ 0.630−1.361 (m, 43H, $-CH_2CH_3$ of BEt_3, CH_2CH_2 of dippe, and CH_3 groups of isopropyl group), 1.461−1.515 (m, 2H, CH), 1.969−2.022 (m, 2H, CH), 2.472 (d, $^4J_{P-H} = 4.8$ Hz, 3H, CH_3CN); ^{31}P{^{1}H}: δ 79.43 (d, $^2J_{P-P} =$ 47 Hz), 63.07 (d, $^2J_{P-P} = 47$ Hz). ^{13}C{^{1}H}: δ 11.6 (s, CH_3CH_2-), 16.2 (m, $B-CH_2CH_3$), 17.3 (dd, CH_3 of CH_3CN), 18.337 (d, CH_3), 19.8 (d, CH_3), 20.178 (d, CH_3), 21.4 (dd, CH_2), 25.0 (d, CH), 25.9 (d, CH), 164.0 (dd, CN).

4.6. Photolysis Experiments. A typical experiment was performed using THF solutions of 100 mg of each complex in J-Young tubes, and the reaction was followed by ^{1}H and ^{31}P NMR spectroscopy. These experiments were carried out on compounds **1** and **5** under nitrogen ($\lambda > 300$ nm), with results as described in the text.

4.7. Crystal Structure Determinations. For each structure determination, a crystal was placed onto the tip of a 0.1 mm diameter glass fiber and mounted on a Bruker SMART APEX II Platform CCD diffractometer for data collection at 100.0(1) K.[29] A preliminary set of cell constants and an orientation matrix were calculated from reflections harvested from three orthogonal sets of 20 frames. The data collections were carried out using Mo Kα radiation (graphite monochromator) with frame times of 10−25 s and a detector distance of 5.0 cm. A randomly oriented region of reciprocal space was surveyed: four major sections of frames were collected with 0.50° steps in ω at four different Φ settings and a detector position of −33° in 2θ. The intensity data were corrected for absorption.[30] Final cell constants were calculated from the *xyz* centroids of a sampling of strong reflections from the actual data collection after integration.[31]

Each structure was solved using SIR97[32] and refined using SHELXL-97.[33] The space groups *Pbca* for **4-Cl** and $P2_12_12_1$ for **5** were determined based on systematic absences and intensity statistics. A direct-methods solution was calculated which provided most non-hydrogen atoms from the E-map. Full-matrix least-squares/difference Fourier cycles were performed which located the remaining non-hydrogen atoms. All non-hydrogen atoms were refined with anisotropic displacement parameters. All hydrogen atoms were placed in ideal positions and refined as riding atoms with relative isotropic displacement parameters. The final full matrix least-squares refinement converged to $R1$ values of 0.0332 for **4-Cl** and 0.0397 for **5** (F^2, $I > 2\sigma(I)$) and $wR2$ values of 0.0831 for **4-Cl** and 0.0843 for **5** (F^2, all data).

Acknowledgment. We would like to acknowledge the DOE for financial support for Ting Li (DE-FG02-866ER13569) and the NSF for financial support for Tülay A. Ateşin (CHE-0414325). We thank Abdurrahman Atesin, Mu-Hyun Baik, Eric Lobenstein, Harry Stern, Clark Landis, and Eric Clot for helpful discussions.

Supporting Information Available: Energy level diagram of MOs for acetonitrile and the [Ni(dmpe)] fragment, gas-phase energy diagram for C−C and C−H bond activation of acetonitrile by [Ni(dmpe)], energies with different functionals, tables of selected natural bond orbitals, their composition, and perturbation theory energies, optimized geometries of the structures **S1**−**S7** as well as the fragments with PCM and in gas phase, and portions of Gaussian input files for the geometry optimizations of structures **S1**−**S7**. A complete reference 22 is also given. Structure reports for **4-Cl** and **5** are included, and crystallographic CIF data have been deposited at the Cambridge Crystallographic Data Centre and allocated the deposition numbers CCDC 634622 and 634623. This material is available free of charge via the Internet at http://pubs.acs.org.

JA0707153

(29) *APEX2 V2.0-2*; Bruker Analytical X-ray Systems: Madison, WI, 2006.
(30) Blessing, R. *Acta Crystallogr*. **1995**, *A51*, 33.
(31) *SAINT V7.23A*; Bruker Analytical X-ray Systems: Madison, WI, 2006.
(32) Altomare, A.; Burla, M. C.; Camalli, M.; Cascarano, G.; Giacovazzo, C.; Guagliardi, A.; Moliterni, A. G. G.; Polidori, G.; Spagna, R. *J. Appl. Crystallogr*. **1999**, *32*, 115.
(33) *SHELXTL V6.14*; Bruker Analytical X-ray Systems: Madison, WI, 2000.